Published in final edited form as:
Dent Mater. 2009 June ; 25(6): 781–790. doi:10.1016/j.dental.2009.01.002.

Graded structures for damage resistant and aesthetic all-ceramic restorations

Yu Zhang* and **Jae-Won Kim**
Department of Biomaterials and Biomimetics, New York University College of Dentistry, New York University, New York, USA

Abstract

Objectives—Clinical studies revealed several performance deficiencies with alumina- and zirconia-based all-ceramic restorations: fracture; poor aesthetic properties of ceramic cores (particularly zirconia cores); and difficulty in achieving a strong ceramic–resin-based cement bond. We aim to address these issues by developing a functionally graded glass/zirconia/glass (G/Z/G) structure with improved damage resistance, aesthetics, and cementation properties.

Methods—Using a glass powder composition developed in our laboratory and a commercial fine zirconia powder, we have successfully fabricated functionally graded G/Z/G structures. The microstructures of G/Z/G were examined utilizing a scanning electron microscopy (SEM). The crystalline phases present in G/Z/G were identified by X-ray diffraction (XRD). Young's modulus and hardness of G/Z/G were derived from nanoindentations. Critical loads for cementation radial fracture in G/Z/G plates (20×20 mm^2, 1.5 or 0.4 mm thick) bonded to polycarbonate substrates were determined by loading with a spherical indenter. Parallel studies were conducted on homogeneous Y-TZP controls.

Results—The G/Z/G structure consists of an outer surface aesthetic glass layer, a graded glass-Y-TZP layer, and a dense Y-TZP interior. The Young's modulus and hardness increase from surface to interior following power-law relations. For G/Z/G plates of 1.5 and 0.4 mm thick, critical loads for cementation radial fracture were 1990±107 N (mean±SD, n = 6) and 227±20 N (mean±SD, n = 6) respectively, which were ~30% and 50% higher than those for their monolithic Y-TZP counterparts (1388±90 N for 1.5 mm and 113±10 N for 0.4 mm thick; mean±SD, n = 6 for each thickness). A 1-sample t-test revealed significant difference ($p < 0.001$) in critical loads for radial fracture of G/Z/G and homogeneous Y-TZP for both specimen thicknesses.

Significance—Our results indicate that functionally graded G/Z/G structures exhibit improved damage resistance, aesthetics, and potentially cementation properties compared to homogeneous Y-TZP.

Keywords

dental ceramic; zirconia; graded structures; aesthetics; damage resistance

*Corresponding author: Yu Zhang, New York University College of Dentistry, Department of Biomaterials and Biomimetics, 345 East 24th Street, Room 813C, New York, NY 10010, USA, Phone: (212) 998-9637; Fax: (212) 995-4244, e-mail: yz21@nyu.edu.

1. Introduction

Teeth play a critically important role in our lives. Loss of function reduces our ability to eat a balanced diet, which has negative consequences for systemic health. Loss of aesthetics can negatively impact social function. Both function and aesthetics can be restored with dental crowns and bridges. Ceramics are attractive dental restoration materials because of their aesthetics, biological acceptance, and chemical durability. However, ceramics are brittle and subject to premature failure, especially under repeated contact loading in a moist environment [1]. Despite a continuous effort in improving the strength of dental ceramics (e.g. using a strong zirconia or alumina core to support a weak but aesthetic porcelain veneer), all-ceramic dental prostheses (including veneered zirconia and alumina restorations) continue to fail at a rate of approximately 1–3% each year [2]. In addition to the fracture problem, veneered zirconia and alumina prostheses have a dense, high purity crystalline structure at the cementation surface that cannot be readily adhesively bonded to tooth dentin support [3,4]. Surface roughening treatment such as particle abrasion is commonly used to enhance the ceramic–resin-based cements bond using mechanical retention [3]. However, particle abrasion also introduces surface flaws or microcracks that can cause deterioration in the long-term flexural strength of ceramic prostheses [5,6]. Further, zirconia cores have a white opaque appearance which needs a thick porcelain veneer with gradual change in translucency (optical properties) to mask the zirconia and to achieve a better aesthetic outcome [7]. The aforementioned problems motivated us to develop novel damage resistant, aesthetic, easy to cement, and ultra strong glass/zirconia/glass structures for all-ceramic prostheses.

The impetus for this assertion comes from previous works by Suresh, Nitin and their team [8,9]. These authors showed that when the contact surface of alumina or silicon nitride was infiltrated with aluminosilicate or oxynitride glass, respectively, which have similar coefficients of thermal expansion (CTEs) and Poisson's ratios but lower moduli to the infiltrating surfaces, an increase in elastic modulus from surface glass to a strong ceramic interior can be engineered without introducing significant residual stresses. The graded glass/ceramic (G/C) surfaces produced in this manner offered much better resistance to contact [8, 10] and sliding [11] damage than either constituent ceramic or glass. We argue that if we extend the G/C system to a graded G/C/G structure by infiltrating the top and bottom ceramic surfaces with glass, the resultant G/C/G system will suppress both contact damage at the occlusal surface and flexural damage at the cementation surface, margins, and lower connector regions of multi-unit bridges. In addition, the unique structure of G/C/G, which includes an outer surface aesthetic residual glass layer, a graded glass-ceramic layer, and a dense ceramic interior, allows us to tailor optical and cementation properties. Since yttria-stabilized tetragonal zirconia polycrystal (Y-TZP) is far superior in mechanical properties compared to other oxides utilized in restorative dentistry, we are focusing on the development of zirconia-based glass/zirconia/glass (G/Z/G) restorative materials.

2. Materials and methods

2.1. Materials

As a first step towards the development of graded Y-TZP structures, a new family of glass in the SiO_2-Al_2O_3-K_2O-Na_2O-CaO-Tb_4O_7 system has been developed to infiltrate Y-TZP. The main composition (> 1 wt.%) of the infiltrating glass contained: SiO_2 (65.5 wt.%), Al_2O_3 (11.7 wt.%), K_2O (10.0 wt.%), Na_2O (7.3 wt.%), CaO (3.0 wt.%), and Tb_4O_7 (1.9 wt.%). This composition was selected so that the final product was highly translucent with a light yellow shade, and had a high melting point coupled with an excellent resistance to crystallization during the cooling from the elevated temperatures. The CTE of the selected glass composition was around $10.4 \times 10^{-6} °C^{-1}$, from 25 – 450°C, similar to that of Y-TZP ($10.5 \times 10^{-6} °C^{-1}$, from 25 – 450°C).

Green compacts were formed from a fine size (d ~ 28 nm) yttria-stabilized zirconia powder (5.18 wt.% Y_2O_3, TZ-3Y-E grade, Tosoh, Tokyo, Japan) using a cold isostatic press at 200 MPa. The green compacts were divided into two groups. To produce monolith Y-TZP, one group was sintered at 1450°C for 2 hrs inside a high temperature box air furnace (ST-1700C-6612, Sentro Tech Corp, Berea, OH). To produce graded structures, another group was presintered between 1100°C to 1400°C for 1 hr in air, producing a somewhat porous template for glass infiltration. The top and bottom surfaces of presintered Y-TZP were coated with a slurry of the aforementioned powdered glass composition. Glass infiltration and densification were carried out simultaneously at 1450°C for 2 hrs in air. This way the glass infiltration depth can be tailored by manipulating the porosity of the infiltrating structures, and the grain growth [12] and/or destabilizing of the tetragonal zirconia phase [13] associated with the post-sintering heat treatment can be prevented. Both grain growth and/or destabilizing of the tetragonal phase are known to be deleterious for hydrothermal stability of Y-TZP in the body [14–16]. A heating and cooling rate of 900°C/hr was employed in all cases.

2.2. Characterization

Microstructures of G/Z/G specimens were examined by a scanning electron microscopy (SEM) (Hitachi 3500N, Japan). Specimens were sectioned using a water cooled low speed diamond saw (Isomet, Buehler, Lake Bluff, IL). The cross sections were polished to 1 μm finish and carbon coated. One of the glass infiltrated surfaces of G/Z/G was subjected to hydrofluoric acid (HF, 10%) etching for 15 minutes to remove the outer surface residual glass layer and to selectively remove the glassy phase in the graded glass-zirconia layer. The etched surfaces were rinsed with deionized water for 5 minutes, dried, and carbon coated for SEM examination.

The crystalline phases present in G/Z/G and homogeneous Y-TZP specimens were identified using an X-ray diffractometer (XRD) (Philips X'Pert System, Almelo, Overijssel, Netherlands) with nickel filtered CuK_α radiation. Scans were performed on the as sintered/infiltrated surface over the 2θ range 15°– 70° at a scanning rate of 1°/min and a step size of 0.02°.

CTEs of the infiltrating glass and Y-TZP were determined using a dilatometer (L75VD1600, LINSEIS, Princeton Junction, NJ). Specimens were prepared in a bar shape: 6 × 6 × 35 mm. A heating and cooling rate of 5°C/min was employed.

2.3. Mechanical testing

Young's modulus and hardness of the residual glass layer, graded glass-zirconia layer and the Y-TZP interior were measured using nanoindentations, carried out on a 3D Omni Probe TriboIndenter (Hysitron, Minneapolis, MN) with a Berkovich indenter. Measurements were made on the polished (1 μm finish) cross sections of G/Z/G at a maximum load of 40 mN to produce a penetration depth of ~0.4 and ~0.6 μm in the dense Y-TZP and glass regions, respectively. Such penetration depths resulted in indentation impressions with lateral dimensions of ~3 – 4 μm. Considering the average grain size of Y-TZP is ~0.5 μm, a lateral indentation impression of 3 μm would probe 15–20 grains in a dense Y-TZP region or over 5 adjacent grains in the graded layer. Nanoindentations were made from the surface residual glass layer, through the graded glass-zirconia layer to the Y-TZP interior with a step size of 3 μm. To ensure the distance between any two indents was greater than the dimension of two indentation impressions, we conducted a line mapping in a direction diagonal to the specimen surface normal; the indenter traveled 15 μm parallel to the surface and 3μm perpendicular to the surface before making the next indent. The Young's modulus and hardness for each indentation were determined from load-displacement curves using the well-documented method of Oliver and Pharr [17,18]. It is important to note that the elastic modulus measured is a reduced modulus E_r. The actual modulus of our graded material, E, was computed using

the relationship proposed by Oliver and Pharr [17]: $\frac{1}{E_r}=\frac{1-\nu^2}{E}+\frac{1-\nu_i{}^2}{E_i}$, where ν is the Poisson's ratio of the ceramic material; E_i and ν_i are the elastic modulus and Poisson's ratio of the diamond indenter. Here we use $\nu = 0.3$ for Y-TZP and for the graded glass-zirconia composite, $E_i = 1040$ GPa and $\nu_i = 0.07$ for the diamond indenter [17].

Resistance to flexure induced radial fracture of G/Z/G was determined by loading the top surface of the G/Z/G/polycarbonate bilayers with a tungsten carbide indenter ($r = 3.18$ mm) mounted onto the cross head of a screw-driven universal tester (Model 5566, Instron Corp., Canton, MA). Flat G/Z/G plates with a surface dimension of 20 × 20 mm were fabricated from presintered Y-TZP plates (1400°C for 1 hr) followed by glass infiltration at 1450°C for 2 hrs. The excess glass was ground away from both the top and bottom surfaces of G/Z/G. The plates were polished (1 μm surface finish) to a thickness of $d = 1.5$ mm or 0.4 mm, and then bonded with epoxy resin (Harcos Chemicals, Bellesville, NJ) onto polycarbonate substrates 12.5 mm thick (Hyzod, AlN Plastics, Norfolk, VA). Parallel studies were conducted on the Y-TZP/polycarbonate bilayers. The load was applied perpendicular to the specimen's surface at a constant rate of 1 mm/min. Six specimens were measured for each group. Fracture was observed *in-situ* using a video camera equipped with a microscope zoom system (Optem, Rochester, NY). The critical loads for onset of the flexure induced bottom surface radial fracture were determined.

3. Results

SEM images of G/Z/G fabricated from presintered bodies (1400°C for 1 hr) followed by glass infiltration/sintering at 1450°C for 2 hrs are shown in Fig. 1. The total thickness of G/Z/G plates was ~1.5 mm, including a thin, outer surface residual glass layer followed by a graded glass-zirconia layer at both the top and bottom surfaces, sandwiching a dense Y-TZP interior. The outer surface residual glass layer, as shown in a low magnification backscattered electron (BSE) image (Fig. 1a), was approximately 50 μm thick at both the top and bottom surfaces. The graded layers contained a relatively high glass content (dark phase in the BSE image Fig. 1b) at the residual glass layer interfaces and gradually transformed to a dense Y-TZP interior (light phase in Fig. 1b, owing to the high atomic weight of Y-TZP relative to the glass phase). A higher magnification BSE image (Fig. 1b) revealed ~45 vol.% glass in the graded layers near the residual glass layer interfaces. Fig. 1d is a secondary electron (SE) micrograph showing the representative features of a HF (10% for 15 mins) etched G/Z/G surface. A 3-dimentional network of glass coated zirconia grains was exposed, creating a surface morphology ideal for silanization and subsequent adhesive resin penetration.

One concern of G/Z/G was the crystallization of glass, both in the surface residual glass layer and in the graded glass-zirconia layer, upon cooling, which could modify the CTE and impair the aesthetics of G/Z/G. For this reason, we formulated a glass composition which exhibits excellent resistance to crystallization upon cooling. XRD analysis of the as infiltrated G/Z/G surfaces revealed a small amount of glass phase in the surface residual glass and graded glass-zirconia layers for specimens presintered between 1100°C and 1400°C for 1 hr, and then infiltrated/sintered at 1450°C for 2 hrs (Figs. 2a and b). Fig. 2c is an XRD spectrum of a HF etched surface of G/Z/G presintered at 1400°C for 1 hr and infiltrated/densified at 1450°C for 2 hrs. There was no detectable secondary crystalline phase present in addition to the metastable tetragonal phase in all cases, at least within the detection limit of XRD (i.e. ~3 vol.%) (Figs. 2a-c). For reference, an XRD spectrum of a sintered (1450°C for 2 hrs) monolith Y-TZP is shown in Fig. 2d. As can be seen, no monoclinic phase was observed in either glass infiltrated, infiltrated and then etched, or monolith Y-TZP specimens.

The dependence of Young's modulus and hardness gradations on the depth (from both top and bottom surfaces to interior) of G/Z/G are shown in Figs. 3a and b. The specimen was presintered at 1400°C for 1 hr, and then glass infiltrated/sintered at 1450°C for 2 hrs. The residual glass layer (d≈50 μm, labeled as zone **I** in Figs. 3a and b) possessed a Young's modulus value of E = 68.3 ± 2.9 (mean ± SD, n = 12) GPa and a hardness value of H = 8.2 ± 0.2 (mean ± SD, n = 12) GPa. For the glass-zirconia graded layer (d≈120 μm, marked as zone **II** in Figs. 3a and b), the Young's modulus and hardness varied from E = 137.2 GPa and H = 10.5 GPa near the residual glass/graded layer interface to E = 212.7 GPa and H = 16.0 GPa near the graded layer/Y-TZP interior boundary. The Y-TZP interior (identified as zone **III** in Figs. 3a and b) exhibited Young's modulus and hardness values of E = 240.8 ± 9.5 (n = 49) and H = 17.6 ± 0.5 (n = 49) GPa, respectively. Note that the n values quoted in parentheses, n = 12 and n = 49, represent number of indents made in the residual glass layer and the Y-TZP interior, respectively, on a G/Z/G sample. The Young's modulus variation in the graded glass-zirconia layer is best described by a power-law relation $E = E_s + E_0 z^k$, where E_s = 74.6 GPa is the elastic modulus at the interface of residual glass and graded layers; E_0 = 327.5 GPa•mm^{-k} is a scale factor; z is the depth from the residual glass/graded layer interface to interior; and k = 0.32 is an empirically derived coefficient.

Ceramic restorations are cemented onto less stiff tooth dentin structures. Upon occlusion, high tensile stresses develop in the ceramic at the cementation interface directly below the loaded area (highlighted by the dashed grey circle in Fig. 4a). If the tensile stress exceeds the bulk strength of the ceramic layer, an internal surface flexural radial crack (**R**) can form. These radial cracks can propagate upward and sideward, leading to catastrophic fracture of the ceramic restorations [19]. In dentistry, radial cracks are clinically evidenced as bulk fracture [20]. For the first approximation, the resistance of ceramic to radial cracking can be experimentally determined by loading the top surface of a flat ceramic layer bonded to a compliant substrate with a hard spherical indenter [1] (Fig. 4b). This ball-on-flat layer test is similar to a three-point-bend test or a biaxial flexural test of a ceramic bar or disc, except here we take additional consideration of the supporting role of a dentin-like base [19,21,22].

Critical loads for the onset of flexure induced radial facture were measured for polished homogeneous Y-TZP and G/Z/G plates (d = 1.5 or 0.4 mm) bonded with epoxy resin onto polycarbonate substrates. The thickness of the epoxy adhesive interlayer was ~20 μm. For the present study, the thickness of the epoxy resin is not critical, because the Young's modulus of epoxy resin is similar to that of the polycarbonate base [23]. Polycarbonate was selected as a support material for the ceramic plates because it is compliant and can be considered a representative for dentin or bone (though its Young's modulus is slightly lower than that of either) and is transparent, permitting direct observation of radial fractures evolving from the bottom surface of the ceramic layer [24]. G/Z/G plates were fabricated from infiltrating presintered Y-TZP (1400°C for 1 hr) with an aforementioned, in-house prepared glass powder at 1450°C for 2 hrs. Six specimens (n = 6) were fabricated from two different batches for each thickness (d = 1.5 or 0.4 mm). A ~10% variation in critical load was observed between the specimens fabricated from the two different batches. As shown in Figs. 4c and d, for 1.5 mm thick specimens, critical loads for G/Z/G (1990 ± 107 N, mean ± SD) were ~30% higher than those for homogeneous Y-TZP (1388 ± 90 N, mean ± SD). However, for 0.4 mm thick specimens, critical loads for G/Z/G (227 ± 20 N, mean ± SD) were almost twice as high as those for homogeneous Y-TZP (113 ± 10 N, mean ± SD), suggesting that the impact of the graded structure on the flexural damage resistance could be more significant for thin (d < 0.5 mm) ceramic prostheses. A 1-sample t-test showed that it was highly unlikely ($p < 0.001$) that a specimen as strong as G/Z/G could have been sampled from the population of homogeneous Y-TZP for both thicknesses.

The appearance of a glass infiltrated Y-TZP (G/Z/G) framework is shown in Fig. 5, along with a monolithic Y-TZP framework. The G/Z/G framework was fabricated by presintering a Y-TZP green compact at 1400°C for 1 hr followed by glass infiltration/sintering at 1450°C for 2 hrs, while the monolithic Y-TZP framework was sintered at 1450°C for 2 hrs. As can be seen, the G/Z/G framework exhibited a glossy appearance with a light yellow shade (Figs. 5c and d), whereas the Y-TZP framework was white and opaque (Figs. 5a and b). In addition, the interior of G/Z/G also contained a residual glass layer and a graded glass-zirconia layer, which could facilitate the etching-silane cementation procedure.

4. Discussion

Using a glass powder developed in our laboratory, we have successfully established infiltration conditions to fabricate G/Z/G structures in the thicknesses necessary for dental applications. Our data shows that G/Z/G exhibits better resistance to flexure induced cementation radial fracture compared to homogeneous Y-TZP (Figs. 4c and d). We propose the following mechanisms for the observed strengthening effect. When a ceramic plate is bonded to a compliant substrate and loaded axially on the top surface with a spherical indenter, the strain (ε) distribution in the ceramic plate along the loading axis is continuous across the plate's cross section and can be described schematically by Fig. 6a. For a homogeneous Y-TZP plate, the Young's modulus is uniform throughout the section. According to Hooke's law, the stress (σ) in the ceramic plate along the loading axis is also continuous (Fig. 6b). The maximum tensile stress, which occurs at the bottom surface of the flexing Y-TZP plate, is responsible for the flexure induced cementation radial fracture. For a graded G/Z/G plate, the strain state is still continuous (Fig. 6c), but the stress is now discontinuous, owing to the gradient in Young's modulus as a function of depth. Nanoindentation studies of G/Z/G show that the Young's modulus increases from the surface to interior following a power-law relation. Accordingly, the stress distribution in G/Z/G can be described by Fig. 6d, with the tensile stress at the bottom surface of the G/Z/G plate now lowered relative to homogeneous zirconia. In addition, the glass infiltrates the surface flaws of Y-TZP, making G/Z/G relatively immune to the surface flaw status compared to homogeneous Y-TZP. As a result, G/Z/G exhibits better resistance to immediate flexural damage than homogeneous Y-TZP.

By controlling the gradient in glass content on the zirconia surface, good optical properties can be achieved. Although the glass-zirconia graded layer has limited translucency due to its high crystalline content, it provides a gradual transition in translucency from the highly translucent surface residual glass layer to the opaque Y-TZP interior, which allows for the optical depth necessary in creating a good aesthetic outcome. For better aesthetics, a thin porcelain veneer with similar compositions to the infiltrated glass can be applied to the outer surface of G/Z/G. This thin veneer could contain the contact damage, provide aesthetics, prevent unwanted wear of opposing natural dentition, and allow for adjustment on the occlusal surface. Any occlusal-surface contact damage can be confined within the thin veneer layer, because cracks are unlikely to propagate from a low modulus, low toughness porcelain to a high modulus, high toughness Y-TZP [25]. The thin veneer concept is supported by the unique structure of G/Z/G, which includes a surface aesthetic residual glass layer, a graded glass-zirconia layer, and an interior Y-TZP layer (Fig. 5). Alternatively, color stains can be applied to the surface of the outer residual glass layer of G/Z/G using a powdered glass slurry that has similar composition to the infiltrated glass. This staining technique has been used on the Empress system to improve the aesthetic outcome of a single color pressed block of glass-ceramic and is well established in aesthetic dentistry [26,27].

The residual glass and the glass containing graded layer on the internal side (intaglio surface) of G/Z/G offer great potential for adhesive bonding using etching-silane techniques rather than the current grit-blasting procedure for cementation of homogeneous zirconia. The residual

glass layer and the glass phase in the graded layer can be selectively removed by HF acid, creating a 3-dimensional surface morphology (Fig. 1d). A strong resin bond can be established by the application of a silane coupling agent followed by the penetration of an adhesive resin into the 3-dimentional surface network. A previous study shows that Y-TZP containing a similar glass infiltrated surface exhibits a marked improvement in adhesive bond strength using standard etching-silane techniques following simulated aging [28]. The merits of the current research over the previous study [28] lie in two aspects. First, the previous study infiltrates a fully sintered Y-TZP using a two-cycle heat-treatment technique at low temperatures (750°C) with a short dwell time (1 min). As a result, no strengthening effect is observed in glass infiltrated zirconia compared to homogeneous zirconia. In the present study, we infiltrate/densify presintered Y-TZP at 1450°C for 2 hrs, establishing a graded glass-zirconia layer with necessary thickness to spread the maximum tensile stresses from the surface into the interior; and secondly, unlike the previous study which infiltrates only the cementation surface of Y-TZP, we infiltrate all accessible surfaces of the zirconia framework (Figs. 5c and d), improving both the aesthetic and cementation properties.

With an increase in resistance to flexural damage, the absence of grit-blasting damage, and the aid of adhesive cementation, the overall strength of the G/Z/G restoration will be much higher than current veneered Y-TZP restorations. This may ultimately lead to the development of ultra strong yet aesthetic ceramics for posterior inlays, onlays, full-coverage crowns, and fixed partial dentures (FPDs), preserving tooth structure by reducing the thicknesses of the veneering porcelain and G/Z/G framework. The current FPDs with Y-TZP frameworks often fracture from the lower portions of the connectors, leading to chipping or delamination of the porcelain veneer. G/Z/G has improved aesthetics, which allows for a FPD design without porcelain veneering in the lower portions of the connectors, improving the flexural damage resistance of PFDs.

Finally, G/Z/G eliminates sharp interfaces in veneered Y-TZP prostheses, which may ordinarily lead to delamination of the porcelain veneer due to the dissimilar thermal and mechanical properties between porcelain and Y-TZP [29,30]. The residual glass at the G/Z/G surfaces acts as an encapsulation layer that could impede water absorption and prevent hydrothermal degradation of the interior Y-TZP [13]. The present glass–zirconia infiltration technique can be readily extended to other ceramic materials such as alumina, alumina-zirconia composites, etc. Such graded structures offer appealing prospects for the design of next-generation structural ceramics with improved damage resistance and functionality for total joint replacements, dental prostheses, aerospace, military, microelectronics, machining, and other engineering applications.

It is well to acknowledge some limitations of the present study. The current flexural tests have been conducted on specimens with polished surfaces, which do not simulate the clinical cases of the HF etched G/Z/G surfaces and machined or grit-blast Y-TZP surfaces. For this, we argue that the elastic gradients lower the tensile stress at the bottom surface of the G/Z/G plate and render G/Z/G more impervious to surface flaws than Y-TZP. In addition, the present flexural specimens have been loaded monotonically to fast fracture, which does not simulate the clinical case of high cycle fatigue loading. It is well established that ceramic radial fractures are susceptible to enhancement from the fatigue processes [5,6,23,24,31], effectively lowering the critical fracture loads in both G/Z/G and Y-TZP. We are currently conducting long-term fatigue studies of G/Z/G with Y-TZP controls. Moreover, the cementation properties, especially the long-term durability of the G/Z/G–resin bond strength following simulated aging as described by Kern and coworkers [4,32], are yet to be determined.

5. Conclusions

We contend that, using a combined glass infiltration/densification technique, G/Z/G with a graded structure can be fabricated. G/Z/G offers better resistance to immediate flexural damage, better aesthetics, and potentially better veneering and cementation properties over homogeneous Y-TZP.

Acknowledgments

Valuable discussions with Prof. Van P. Thompson and Dr. Brian R. Lawn are appreciated. Thanks are due to Drs. Sanjit Bhomwick and Yvonne Gerbig for conducting nanoindentation measurements, and Dr. Malvin Janal for performing statistic analysis. This investigation was supported in part by Research Grant 5R01 DE017925-2 (PI. Zhang) from the United States National Institute of Dental & Craniofacial Research, National Institutes of Health and Research Grant CMMI-0758530 (PI. Zhang) from the United States Division of Civil, Mechanical & Manufacturing Innovation, National Science Foundation.

References

1. Lawn BR, Deng Y, Thompson VP. Use of contact testing in the characterization and design of all-ceramic crownlike layer structures: a review. J Prosthet Dent 2001 Nov;86(5):495–510. [PubMed: 11725278]
2. Burke FJ, Fleming GJ, Nathanson D, Marquis PM. Are Adhesive Technologies Needed to Support Ceramics? An Assessment of the Current Evidence. J Adhes Dent 2002;4(1):7–22. [PubMed: 12071631]
3. Blatz MB, Sadan A, Kern M. Resin-ceramic bonding: a review of the literature. J Prosthet Dent 2003 Mar;89(3):268–274. [PubMed: 12644802]
4. Kern M, Wegner SM. Bonding to zirconia ceramic: adhesion methods and their durability. Dent Mater 1998 Jan;14(1):64–71. [PubMed: 9972153]
5. Zhang Y, Lawn BR, Malament KA, Van Thompson P, Rekow ED. Damage accumulation and fatigue life of particle-abraded ceramics. Int J Prosthodont 2006 Sep-Oct;19(5):442–448. [PubMed: 17323721]
6. Zhang Y, Lawn BR, Rekow ED, Thompson VP. Effect of sandblasting on the long-term performance of dental ceramics. J Biomed Mater Res B Appl Biomater 2004 Nov 15;71(2):381–386. [PubMed: 15386395]
7. Sailer I, Holderegger C, Jung RE, Suter A, Thievent B, Pietrobon N, et al. Clinical study of the color stability of veneering ceramics for zirconia frameworks. Int J Prosthodont 2007 May-Jun;20(3):263–269. [PubMed: 17580458]
8. Jitcharoen J, Padture NP. Hertzian-Crack Suppression in Ceramics with Elastic-Modulus-Graded Surfaces. J Am Ceram Soc 1998;81(9):2301–2308.
9. Suresh S, Giannakopoulos AE, Alcala J. Spherical Indentation of Compositionally Graded Materials: Theory and Experiments. Acta Materialia 1997;45(4):1307–1321.
10. Pender DC, Padture NP, Giannakopoulos AE, Suresh S. Gradients in elastic modulus for improved contact-damage resistance. Part I: The silicon nitride–oxynitride glass system. Acta Materialia 2001;49(16):3255–3262.
11. Suresh S, Olsson M, Giannakopoulos AE, Padture NP, Jitcharoen J. Engineering the Resistance to Sliding-Contact Damage Through Controlled Gradients in Elastic Properties at Contact Surfaces. Acta Materialia 1999;47(14):3915–3926.
12. Kingery, WD.; Bowen, HK.; Uhlmann, DR. Introduction to Ceramics. Vol. 2. New York: John Wiley; 1976.
13. Piascik JR, Thompson JY, Bower CA, Stoner BR. Stress evolution as a function of substrate bias in rf magnetron sputtered yttria-stabilized zirconia films. Journal of Vacuum Science & Technology A 2006 Jul-Aug;24(4):1091–1095.
14. Chevalier J. What Future for Zirconia as a Biomaterial? Biomaterials 2006;27:534–543.
15. Chevalier J, Cales B, Drouin JM. Low-Temperature Aging of Y-YZP Ceramics. Journal of the American Ceramic Society 1999;82(8):2150–2154.

16. Piconi C, Maccauro G. Zirconia as a ceramic biomaterial. Biomaterials 1999 Jan;20(1):1–25. [PubMed: 9916767]

17. Oliver WC, Pharr GM. An Improved Technique for Determining Hardness and Elastic-Modulus Using Load and Displacement Sensing Indentation Experiments. Journal of Materials Research 1992;7(6):1564–1583.

18. Oliver WC, Pharr GM. Measurement of Hardness and Elastic Modulus by Instrumented Indentation: Advances in Understanding and Refinements to Methodology. Journal of Materials Research 2004;19(1):3–20.

19. Zhang Y, Kim JW, Bhowmick S, Thompson VP, Rekow ED. Competition of fracture mechanisms in monolithic dental ceramics: Flat model systems. J Biomed Mater Res B Appl Biomater. 13 May; 2008 published online

20. Kelly JR. Clinically Relevant Approach to Failure Testing of All-Ceramic Restorations. The Journal of Prosthetic Dentistry 1999;81(6):652–661. [PubMed: 10347352]

21. Lawn BR, Bhowmick S, Bush MB, Qasim T, Rekow ED, Zhang Y. Failure Modes in Ceramic-Based Layer Structures: A Basis for Materials Design of Dental Crowns. Journal of the American Ceramic Society 2007;90(6):1671–1683.

22. Lawn BR, Deng Y, Miranda P, Pajares A, Chai H, Kim DK. Overview: Damage in Brittle Layer Structures From Concentrated Loads. Journal of Materials Research 2002;17(12):3019–3036.

23. Zhang Y, Lawn B. Long-term strength of ceramics for biomedical applications. J Biomed Mater Res B Appl Biomater 2004 May 15;69(2):166–172. [PubMed: 15116406]

24. Zhang Y, Pajares A, Lawn BR. Fatigue and damage tolerance of Y-TZP ceramics in layered biomechanical systems. J Biomed Mater Res B Appl Biomater 2004 Oct 15;71(1):166–171. [PubMed: 15368241]

25. Kim JW, Bhowmick S, Hermann I, Lawn BR. Transverse fracture of brittle bilayers: relevance to failure of all-ceramic dental crowns. J Biomed Mater Res B Appl Biomater 2006 Oct;79(1):58–65. [PubMed: 16470832]

26. Dong JK, Luthy H, Wohlwend A, Scharer P. Heat-pressed ceramics: technology and strength. Int J Prosthodont 1992 Jan-Feb;5(1):9–16. [PubMed: 1520450]

27. Luthy H, Dong JK, Wohlwend A, Scharer P. Effects of veneering and glazing on the strength of heat-pressed ceramics. Schweiz Monatsschr Zahnmed 1993;103(10):1257–1260. [PubMed: 8235523]

28. Aboushelib MN, Kleverlaan CJ, Feilzer AJ. Selective infiltration-etching technique for a strong and durable bond of resin cements to zirconia-based materials. The Journal of Prosthetic Dentistry 2007;98(5):379–388. [PubMed: 18021827]

29. Sundh A, Molin M, Sjogren G. Fracture Resistance of Yttrium Oxide Partially-Stabilized Zirconia All-Ceramic Bridges after Veneering and Mechanical Fatigue Testing. Dental Materials 2005;21:476–482. [PubMed: 15826705]

30. Vult von Steyern P, Ebbesson S, Holmgren J, Haag P, Nilner K. Fracture strength of two oxide ceramic crown systems after cyclic pre-loading and thermocycling. J Oral Rehabil 2006 Sep;33(9):682–689. [PubMed: 16922742]

31. Zhang Y, Lawn BR. Fatigue sensitivity of Y-TZP to microscale sharp-contact flaws. J Biomed Mater Res B Appl Biomater 2005 Feb 15;72(2):388–392. [PubMed: 15551260]

32. Wegner SM, Kern M. Long-term resin bond strength to zirconia ceramic. J Adhes Dent 2000 Summer; 2(2):139–147. [PubMed: 11317401]

33. Krejci I, Albert P, Lutz F. The influence of antagonist standardization on wear. J Dent Res 1999 Feb; 78(2):713–719. [PubMed: 10029471]

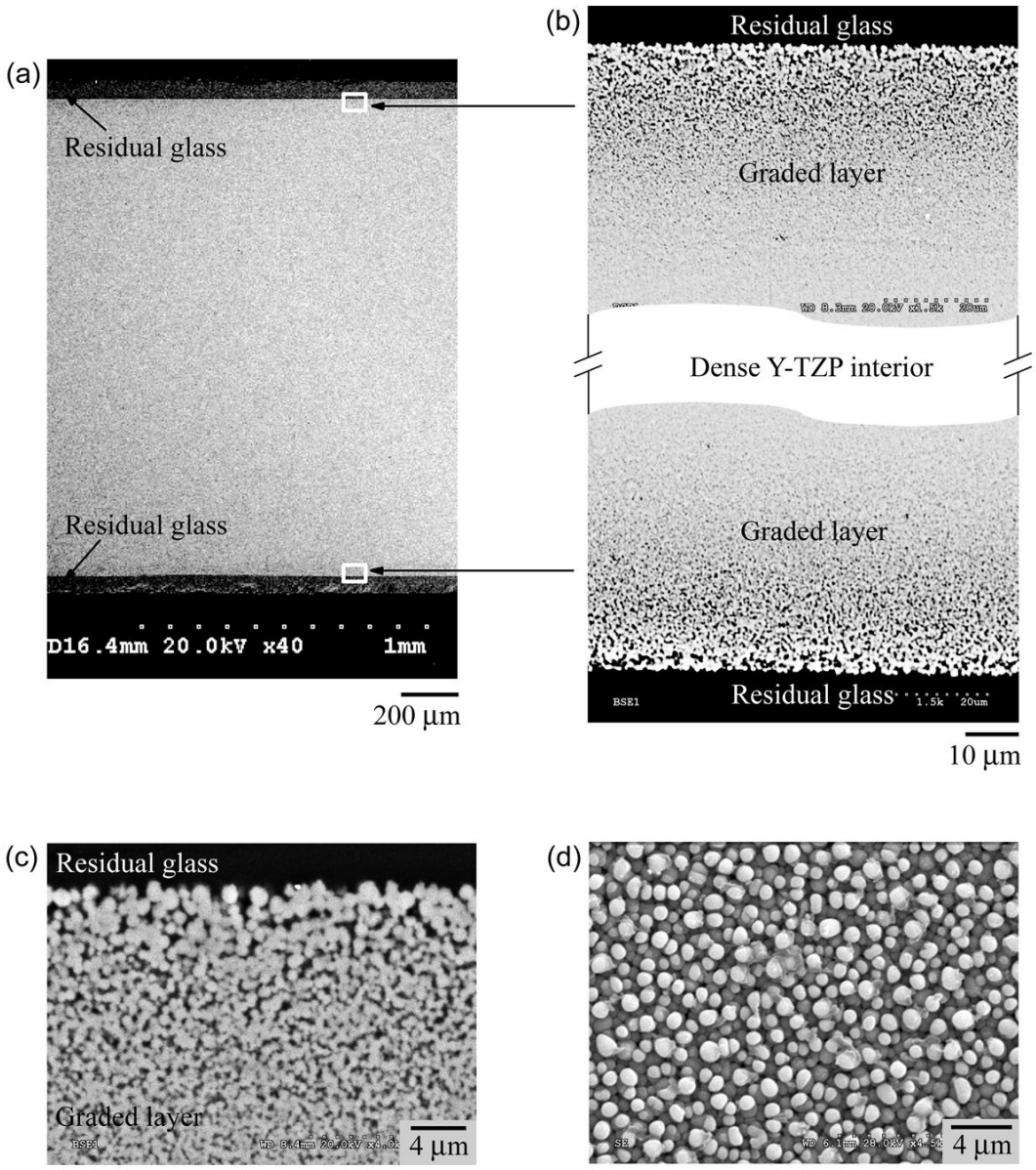

Figure 1.

Scanning electron microscope (SEM) images showing cross-section (polished) and surface (etched) views of G/Z/G (d = 1.5 mm) fabricated from Y-TZP plates presintered at 1400°C for 1 hr followed by glass infiltration/densification at 1450°C for 2 hrs in air. (a) A low magnification backscattered electron (BSE) image revealing cross-sectional features of G/Z/G: an outer surface residual glass layer (~50 µm thick) at both the top and bottom surfaces. (b) Inserts (white boxes) of (a) are BSE images showing outer surface residual glass layer (black), graded glass-zirconia layer, and dense Y-TZP interior. Note: the glass content (black) gradually decreases as proceeding towards the interior. (c) A higher magnification BSE image of (b) revealing (from top down): an outer surface residual glass layer and a graded glass-zirconia layer. (d) A secondary electron (SE) image of a G/Z/G surface subjected to hydrofluoric acid (10%) etching for 15 mins, revealing a 3-dimentional morphology consisting of exposed glass coated zirconia grains, traces of residual glass, and intergranular voids which are ideal for

silanization and subsequent adhesive resin penetration, providing a strong chemical-mechanical bond.

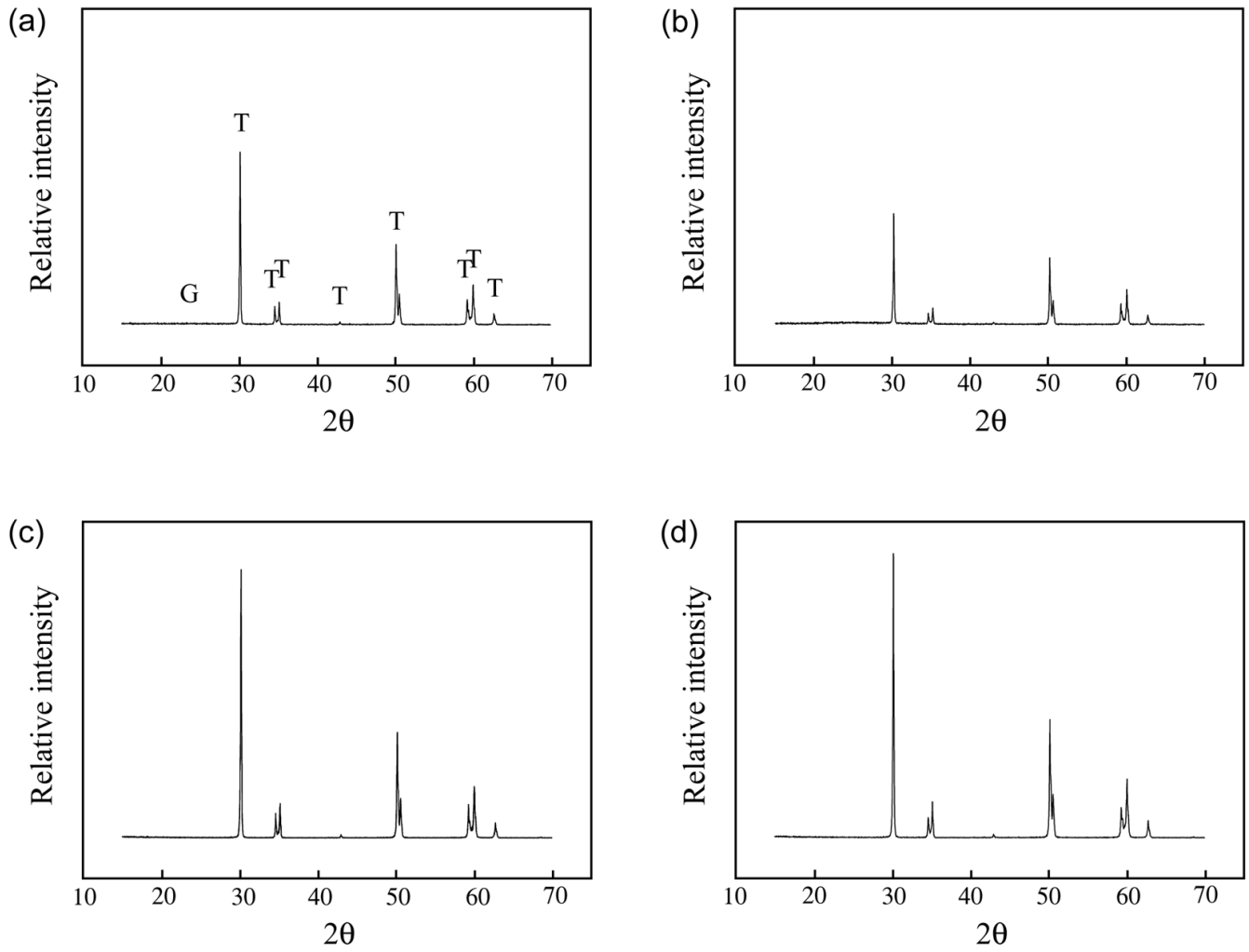

Figure 2.

X-ray diffraction (XRD) spectra of G/Z/G surfaces. (a) and (b) As infiltrated surfaces of G/Z/G fabricated from Y-TZP plates presintered at 1100°C and 1400°C respectively for 1 hr. Glass infiltration and densification were carried out at 1450°C for 2 hrs in air. (c) Hydrofluoric acid (10%, 15 mins) etched surface of G/Z/G fabricated from 1400°C presintered Y-TZP. (d) As sintered surface of homogeneous Y-TZP control sintered at 1450°C for 2 hrs. T: tetragonal zirconia phase, and G: amorphous glass phase. Note: no secondary crystalline phase exists in G/Z/G.

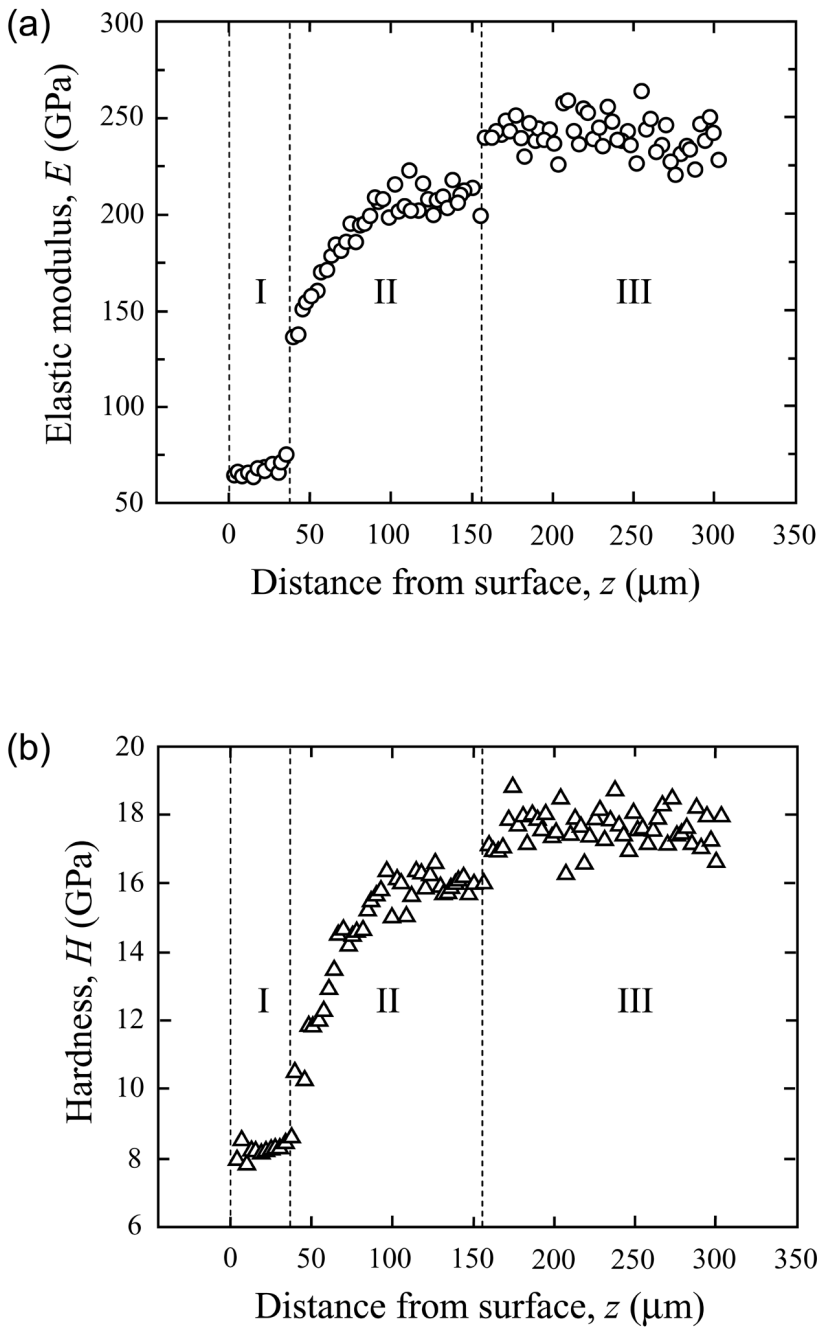

Figure 3.

Variations of (a) Young's modulus *E* and (b) hardness *H* as a function of depth *z* below the G/Z/G surface. G/Z/G specimens were fabricated from presintered Y-TZP plates (1400°C for 1 hr) followed by glass infiltration at 1450°C for 2 hrs. Three distinctive zones are apparent: an outer surface residual glass layer (I), a graded glass-zirconia layer (II), and a dense Y-TZP interior (III).

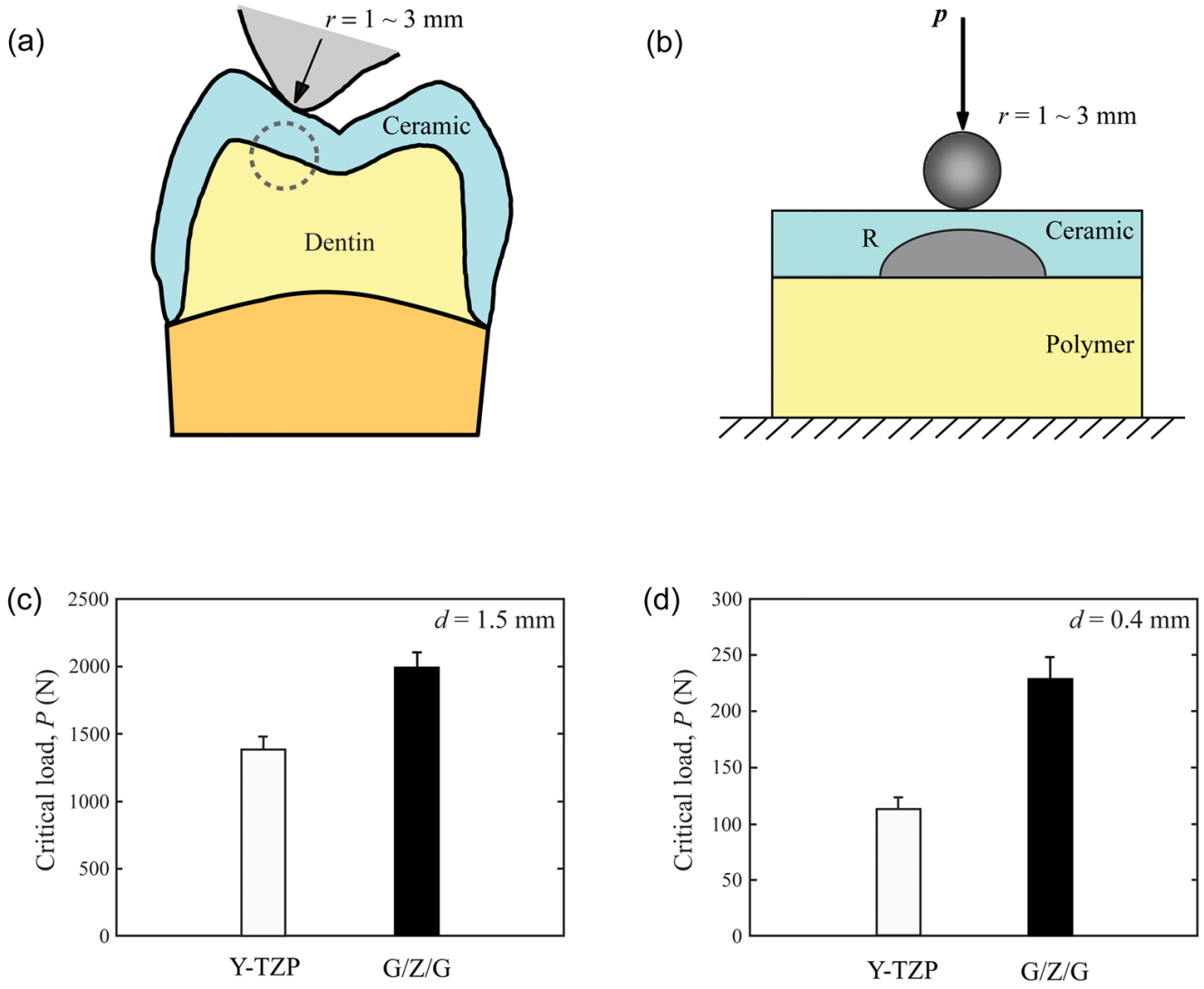

Figure 4.

Ceramic restorations are fully supported by and often bonded to a less stiff dentin. (a) Posterior tooth-to-tooth contact involves contact of the cusp's inner incline with the opposing tooth cusp tip ($r \approx 1$ mm [33]); thus tensile stresses develop directly below the contact area (highlighted by the dashed grey circle). (b) Schematic of Hertzian indentation on flat ceramic/polymer bilayers to determine the resistance of ceramic plates to cementation surface radial cracking. (c) and (d) Bar charts showing critical loads for cementation surface radial cracking in ceramic plates, $d = 1.5$ mm and 0.4 mm respectively, on polycarbonate substrates. Ceramic plates are G/Z/G fabricated from glass infiltration of 1400°C presintered Y-TZP and the homogeneous Y-TZP controls. Note: the advantage of G/Z/G over homogeneous Y-TZP is more pronounced for thinner specimens.

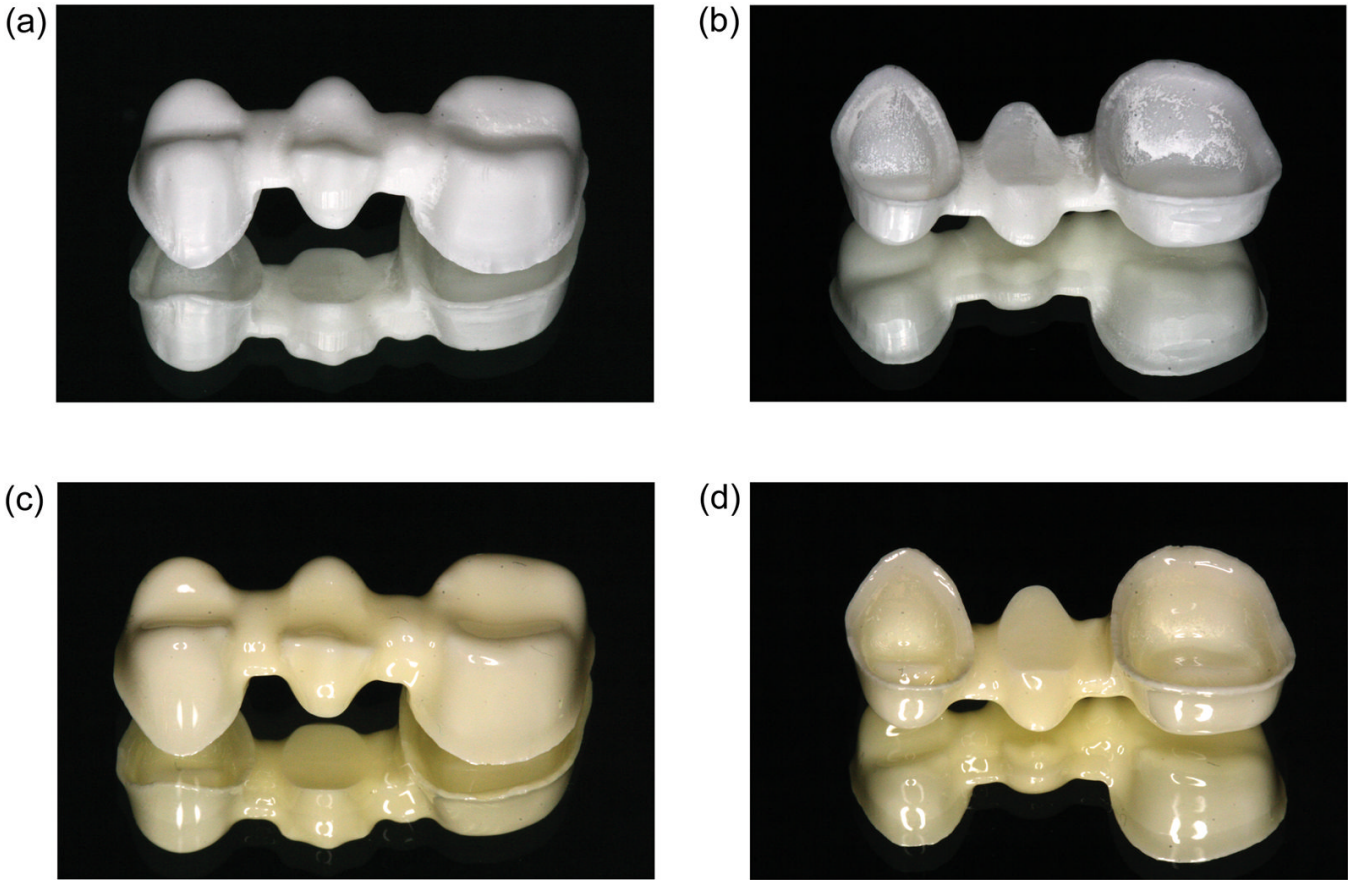

Figure 5.
Digital photographs showing (a) veneering and (b) cementation (intaglio) surfaces of a three-unit Y-TZP framework, and (c) veneering and (d) cementation (intaglio) surfaces of a three-unit G/Z/G framework fabricated from a presintered Y-TZP framework (1400°C for 1 hr) followed by glass infiltration at 1450°C for 2 hrs. Note in (c) and (d): the residual glass layer and the graded glass-zirconia layer at the accessible surfaces of the G/Z/G framework improve both the aesthetic and cementation properties.

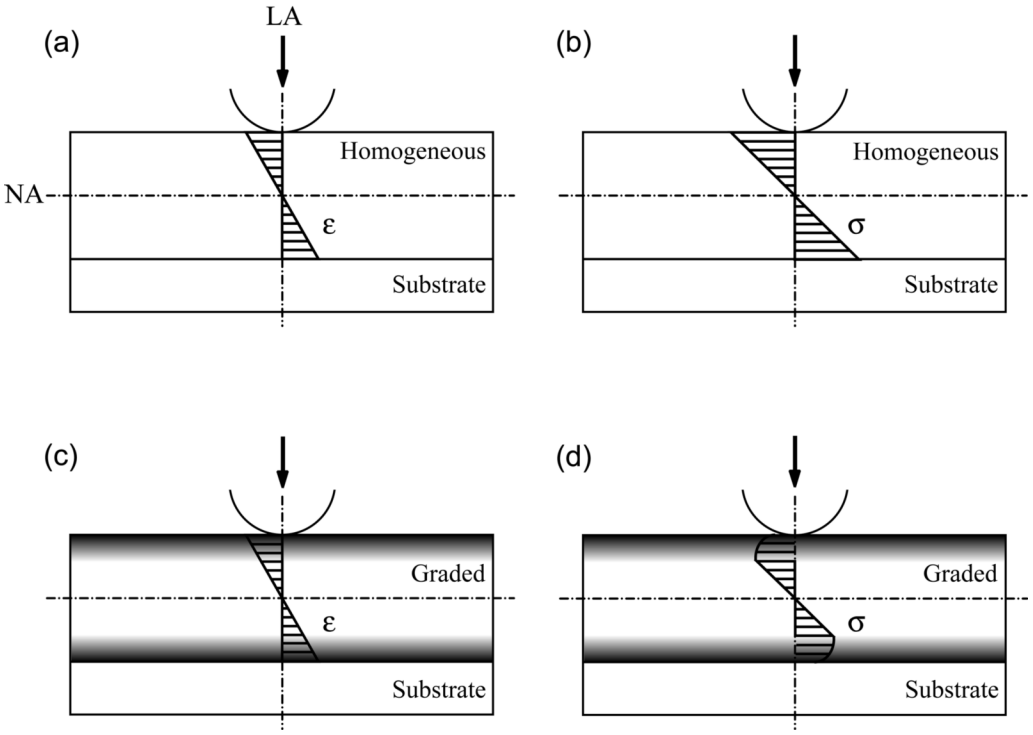

Figure 6.

Schematic demonstrating the strain (ε) and stress (σ) distributions in a ceramic plate on a compliant substrate, loaded axially from the top surface with a hard spherical indenter. Illustrations are made for (a) strain and (b) stress distributions in a homogeneous Y-TZP plate, and (c) strain and (d) stress distributions in a graded G/Z/G plate on compliant substrates along the loading axis across the plate cross section. LA and NA stand for load axis and neutral axis, respectively. Note in (d): the maximum tensile stress at the bottom surface of the G/Z/G plate is lowered relative to homogeneous zirconia (b).